

Deposition of general ellipsoidal particles

Reza M. Baram^{1,*} and Pedro G. Lind^{1,2,†}

¹Center for Theoretical and Computational Physics, University of Lisbon, Av. Prof. Gama Pinto 2, 1649-003 Lisboa, Portugal

²Department of Physics, Faculty of Sciences of the University of Lisbon, 1649-003 Lisboa, Portugal

(Dated: May 28, 2022)

We present a systematic overview of granular deposits composed of ellipsoidal particles with different particle shapes and size polydispersities. We study the density and anisotropy of such deposits as functions of size polydispersity and two shape parameters that fully describe the shape of a general ellipsoid. Our results show that, while shape influences significantly the macroscopic properties of the deposits, polydispersity plays apparently a secondary role. The density attains a maximum for a particular family of non-symmetrical ellipsoids, larger than the density observed for prolate or oblate ellipsoids. As for anisotropy measures, the contact forces show are increasingly preferred along the vertical direction as the shape of the particles deviates for a sphere. The deposits are constructed by means of an efficient molecular dynamics method, where the contact forces are efficiently and accurately computed. The main results are discussed in the light of applications for porous media models and sedimentation processes.

PACS numbers: 81.05.Rm, 45.70.-n, 05.20.-y, 45.70.Cc

Keywords: Packing, Ellipsoidal, Deposition, Porous media

I. INTRODUCTION

The granular character of many processes in nature has motivated the study of granular materials and in particular granular packings since Kepler's time[1]. One of such processes is the deposition of particles subject to gravity[2], which underlies the formation of sandstones, ceramics and in general, the emergence of porous materials. Modelling porous media[4, 5] in a realistic way is important for instance to understand permeability of soils for petroleum engineering or in material sciences.

However, a model for grain deposition should incorporate two ingredients not always easy to combine. First, empirical studies[6] show that the shape of grains significantly deviates from the sphere with a non-negligible polydispersity in their sizes. Until recently most computational studies dealt with round particles for simplicity, in solving specific problems such as obtaining the optimal packing[7, 8], constructing space-filling configurations[9–11] or studying elongated shapes[3]. Some progress was recently made when addressing the influence of particle shape on the macroscopic observables of the agglomerate, focusing on ellipsoidal particles[12, 13] and even in more general shapes[14, 15], without accounting for the size polydispersity.

Second, deposition processes are fundamentally sequential and therefore should be modelled through sequential procedures. The procedure introduced by Donev *et al*[1, 12] for jammed configurations, captures some of the general features observed in granular deposits, such as their density and average coordination number, although it is based on a non-sequential procedure. However, deposition under gravity does not generally lead to a jammed state. Recently, some sequential procedures were already carried out in two-dimensional

deposits of mono-disperse elongated particles[2, 3].

In this paper we focus on three-dimensional polydisperse deposits of general ellipsoids and study how macroscopic properties of such deposits depend on the shape and size polydispersity of particles. We show that the density and coordination number of deposits behaves similarly to what is observed in jammed systems. However, in contrast with randomly constructed jammed systems, deposits become strongly anisotropic when the shape of the particles deviate from the sphere. Furthermore, we find that the size polydispersity plays a minor role when compared to the shape.

To this end, we develop an efficient algorithm for the calculation of the interactions forces at all contact points within a three-dimensional deposits of polydisperse ellipsoids and use it in a Molecular Dynamics[16, 17] method to perform our simulations. Further, we introduce two shape parameters which describe any ellipsoid, enabling a systematic study of the role of particle shape in granular deposits.

The outline of the paper is as follows. In Sec. II we describe the algorithm for calculating the contact forces between colliding ellipsoids with arbitrary size and shape as well as the simulation setup. In Sec. III the control parameters describing the polydispersity in the size and the shape of a general ellipsoid are introduced. In Sec. IV the dependency of macroscopic observables taken from the entire deposit are studied as functions of the control parameters. We focus on the density, coordination number and anisotropy of the deposits. Discussion and conclusions are given in Sec. V.

II. MODELING THE CONTACT FORCES BETWEEN ELLIPSOIDAL PARTICLES

When dealing with large systems, calculating the inter-particle forces is by far the most time consuming part of the computations. This is due to the fact that, in general, every particle can interact with every other one. In granular materials, however, the inter-particle forces are short range making

*Electronic address: reza@cii.fc.ul.pt

†Electronic address: plind@cii.fc.ul.pt

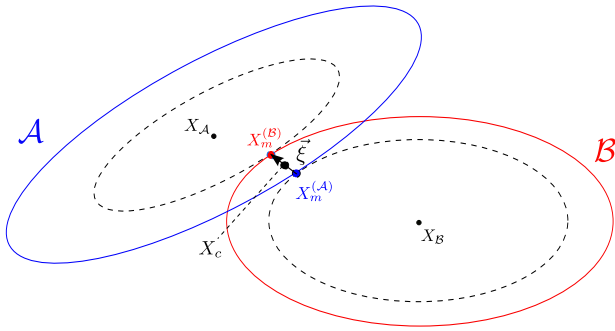


FIG. 1: (Color online) Sketch of the contact vector $\vec{\xi}$ used to define the normal repulsive force between two overlapping ellipsoids \mathcal{A} and \mathcal{B} . The contact point is chosen to be X_c after properly deriving points $X_m^{(A)}$ and $X_m^{(B)}$ at the surfaces of the ellipsoids (see text). The full procedure is sketched in Fig. 2.

techniques such as verlet list and linked-cell algorithm indispensable in reducing the computation time. These techniques are employed to eliminate the redundant calculations for pairs which are too far apart to have any interaction[16].

In time-driven Molecular Dynamics (MD) methods of granular materials the system is evolved for one time step allowing the particles to overlap. Then normal repulsion forces on the particles are calculated as a function of the amount of overlapping, which is defined usually by a line segment. Here we refer to this line segment as the contact vector (see Fig. 1).

The contact vector between two ellipsoids can be defined in more than one way. The common method, introduced by Peram and co-workers[18] and developed by others[13, 19, 20], is based on finding two points, one on the surface of each ellipsoid by minimizing a potential through a variational problem with one geometric constraint. The two obtained points can be used to define the contact vector. However, the contact vector defined this way is not necessarily normal to the surface of the particles, particularly when particles are strongly asymmetrical, leading to non-physical motions of the particles.

An alternative method consists in finding two points on the surfaces of the ellipsoids at which the corresponding surface normals point exactly in opposite directions. Consequently, the vector connecting these two points is normal to the surfaces of both ellipsoids and can be used as a well-defined contact vector. This method is, however, much more computationally expensive than the former one. See Ref. [21] for more details.

To retain the computational efficiency, we use the former method and introduce an additional step for correcting the direction of the contact vector.

The geometric potential of the ellipsoid \mathcal{A} is defined as:

$$f_{\mathcal{A}}(X) = (X - X_{\mathcal{A}})^T \mathbf{A}(X - X_{\mathcal{A}}), \quad (1)$$

where X and $X_{\mathcal{A}}$ are the Cartesian coordinates of a point on the surface and the centroid of the ellipsoid, respectively. The equation $f_{\mathcal{A}}(X) = 1$ describes the surface of ellipsoid \mathcal{A} . Considering a pair of ellipsoids \mathcal{A} and \mathcal{B} , two minimum points $X_m^{(A)}$ and $X_m^{(B)}$ are found on the surfaces of \mathcal{A} and \mathcal{B} by

minimizing $f_{\mathcal{B}}$ and $f_{\mathcal{A}}$, respectively. These points are shown schematically in Fig.1. To obtain the minima of $f_{\mathcal{A}}(X)$ subject to the constraint of being on the surface of ellipsoid \mathcal{B} we minimize the following auxiliary potential:

$$f(X) = (X - X_{\mathcal{A}})^T \mathbf{A}(X - X_{\mathcal{A}}) + \lambda [(X - X_{\mathcal{B}})^T \mathbf{B}(X - X_{\mathcal{B}}) - 1], \quad (2)$$

where λ is the Lagrange multiplier associated with the constraint. Setting to zero the gradient of this function with respect to X ,

$$\nabla f(X) = \mathbf{A}(X_m - X_{\mathcal{A}}) + \lambda \mathbf{B}(X_m - X_{\mathcal{B}}) = 0, \quad (3)$$

we obtain an equation for *optimum* points X_m for \mathcal{A} :

$$X_m = (\mathbf{A} + \lambda \mathbf{B})^{-1} (\mathbf{A} X_{\mathcal{A}} + \lambda \mathbf{B} X_{\mathcal{B}}). \quad (4)$$

To derive an equation for λ we left-multiply Eq. (3) by $(X_m - X_{\mathcal{B}})^T$ and use the fact that X_m lies on \mathcal{B} and that the gradients of the potential functions of the ellipsoids at *minimum* point are in opposite directions:

$$\lambda = |(X_m - X_{\mathcal{B}})^T \mathbf{A}(X_m - X_{\mathcal{A}})|. \quad (5)$$

Equations (4) and (5) can be solved iteratively to find $X_m^{(A)}$ up to the desired precision. The second point $X_m^{(B)}$ can be found similarly.

The contact point X_c where a contact force is exerted on both ellipsoids is defined as the midpoint between $X_m^{(A)}$ and $X_m^{(B)}$. The contact vector for ellipsoid \mathcal{A} is defined as $\vec{\xi}_{\mathcal{A}} = X_m^{(A)} - X_m^{(B)}$ and for ellipsoid \mathcal{B} , $\vec{\xi}_{\mathcal{B}} = -\vec{\xi}_{\mathcal{A}}$ (see Fig. 1).

Although Eq. (4) involves inversion of a 3×3 -matrix, finding the minima can be very efficient by choosing the initial points properly. Good approximations for minima are the minima from the last time step or, if the ellipsoids were disjoint in the last time step, the closest points on the surfaces of the ellipsoids which are known from collision detection procedure described later in this section. These points are then used as initial points, reducing the number of iterations significantly.

The overlapping vector calculated in this way, however, is not necessarily normal to the ellipsoids at the contact point. In fact, the normal directions to \mathcal{A} and \mathcal{B} at points $X_m^{(A)}$ and $X_m^{(B)}$ deviate significantly from each other when the particles are strongly aspherical. To overcome this problem we introduce an additional step for correcting the contact vector, as described next.

If the calculated contact vectors deviate more than a given amount from the gradients of the ellipsoid's potential at the contact point X_c , a new direction is calculated by averaging the gradients at X_c . Then, two new points are calculated from the intersection of the line along this direction passing through the contact point. These new points are used to define a new contact vector. Although it is not generally possible to define a vector which is along the gradients of both ellipsoids at the contact point, this approximation gives satisfactory results in terms of energy conservation.

Having described the procedure for calculating the contact of two colliding ellipsoids, we next need an efficient way to

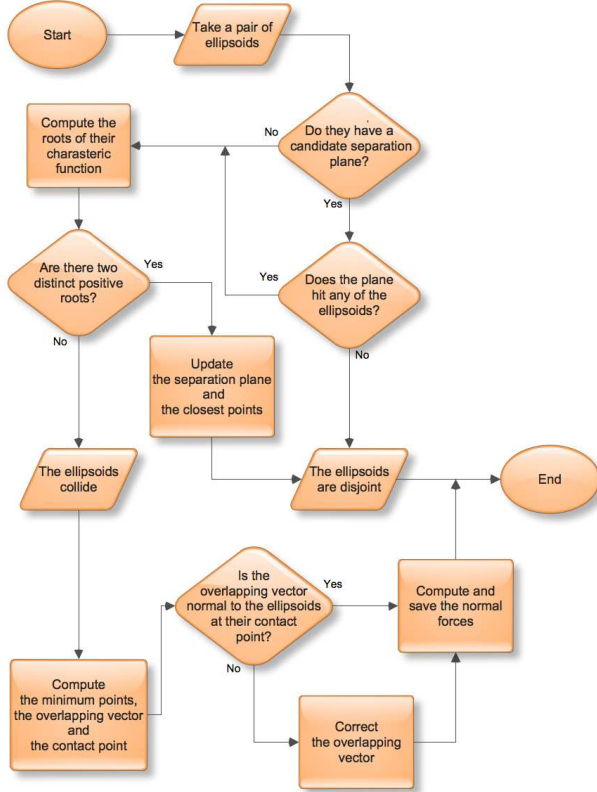


FIG. 2: (Color online) Flow-chart of the algorithm for detection and calculation of the contact points between two arbitrary ellipsoids.

determine when two previously disjoint ellipsoids collide. To this end, we use the technique proposed by Wang *et al*[25] which is described briefly as follows.

In homogeneous coordinates the equation for the surface of a general ellipsoid is given by

$$\mathbf{A} : X^T \mathbf{A} X = 0, \quad (6)$$

where X is any point on the surface of the ellipsoid and \mathbf{A} is the 4×4 -matrix of the affine transformation which transforms the unit sphere centered at the origin into the ellipsoid.

Given two ellipsoids $\mathcal{A} : X^T \mathbf{A} X = 0$ and $\mathcal{B} : X^T \mathbf{B} X = 0$, their characteristic equation is defined as $f(\nu) = \det(\nu \mathbf{A} + \mathbf{B})$, whose roots are the eigenvalues of matrix $-\mathbf{A}^{-1} \mathbf{B}$. Furthermore, it can be shown [25] that (i) $f(\nu) = 0$ has at least two negative roots, (ii) $f(\nu) = 0$ has two distinct positive roots if and only if the two ellipsoids are disjoint, (iii) $f(\nu) = 0$ has a positive double root if and only if the two ellipsoids are externally touching. Therefore, by examining the eigenvalues of $-\mathbf{A}^{-1} \mathbf{B}$ it can be determined if two ellipsoids collide.

When the ellipsoids are disjoint, the corresponding eigenvectors give the coordinates of the four vertices V_i , $i =$

$1, \dots, 4$, of a tetrahedron which is self-polar for both ellipsoids \mathcal{A} and \mathcal{B} [26], i.e. $V_i^T \mathbf{A} V_j = V_i^T \mathbf{B} V_j = 0, \forall i \neq j$. Two of the vertices lie outside both ellipsoids (external vertices), while the other two are contained inside the ellipsoids, one in each (internal vertices). In this case, a set of separation planes can be defined using three points exterior to both ellipsoids, two of them being the external vertices and the other a point on the line segment connecting the internal vertices. We choose the third point as the midpoint between the surfaces of two ellipsoids on this line segment.

Having the separation plane between the two disjoint ellipsoids, in the subsequent time step we check if the ellipsoids intersect that plane. If not, the ellipsoids are still disjoint and the procedure stops. This helps to eliminate the need for checking for collision between the ellipsoids which is more computationally expensive. Only when any of the ellipsoids intersects the separation plane it is necessary to check again for the collision between the ellipsoids. If the ellipsoids turn out to be still disjoint their separation plane and closest points are updated to be used in the next time step. If the ellipsoids do collide the contact vector is calculated and saved to be used for the calculation of the contact force.

Figure 2 shows the flow-chart of the complete procedure which is performed for all potentially overlapping pairs of ellipsoids. It is worth noting that, to further speed up the procedure, only the pairs whose spherical envelopes intersect are evaluated.

The contact force can be decomposed to normal and tangential forces. The tangential forces such as static and dynamical frictions are generally derived from the normal force. For calculating the magnitude of the normal force we use Hertzian model[16]:

$$F_n \propto \xi^{3/2} + K \sqrt{\xi} \frac{d\xi}{dt}, \quad (7)$$

with $\xi = |\vec{\xi}|$ being the length of the contact vector between the particles and K being the dissipative constant depending on the material viscosity [22]. Since we are only concerned with the properties of the deposit at rest, we choose K sufficiently large for the deposit to relax rapidly. This relaxation is enhanced by including a tangential force $\vec{F}_t = \mu F_n \vec{v}_t$, μ being the dynamic friction coefficient and \vec{v}_t the relative tangent velocity of the particles.

Finally, the procedure described above is used in a MD simulation together with standard methods, namely a prediction-correction integrator for solving the equations of motions, quaternions for describing the orientation of the particles and linked-cell algorithm to eliminate unnecessary collision detections. For details of the MD methods see e.g. Ref. [16] and references therein.

III. CONTROL PARAMETERS FOR SIZE AND SHAPE

The size and shape of the particles are the main parameters whose effects on the properties of the system are to be studied. In the following we explain how these are defined and chosen when preparing the samples.

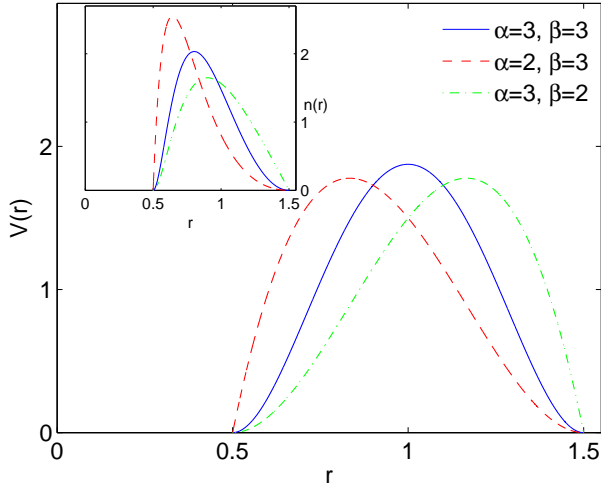


FIG. 3: Volume distributions $V(r)$ for different values of α and β as defined in Eq. (8). The inset shows the corresponding size distributions $n(r)$ (see text).

We define the size of an ellipsoidal particle as the radius of the sphere with the same volume, i.e. $r = (abc)^{\frac{1}{3}}$ with a , b and c being the three semi-axis radii of the ellipsoid. We refer to a sample as mono-sized or monodisperse in size when all its constituting particles have the same volume, i.e. the same size r . To introduce size polydispersity we adopt the approach by Voivret *et al*[23]: instead of directly choosing the size distribution $n(r)$ of the particles, we consider the distribution of the total volume $V(r) = \frac{4}{3}\pi n(r)r^3$ of all particles with size r .

We chose $V(r)$ as

$$V(r) = \begin{cases} C \frac{(r-r_{min})^{\alpha-1}}{(r_{max}-r)^{1-\beta}} & \text{if } r_{min} \leq r \leq r_{max} \\ 0 & \text{otherwise,} \end{cases} \quad (8)$$

where α and β determine the shape of the distribution and C is the normalization factor. Figure 3 shows $V(r)$ for different values of α and β and the corresponding size distributions $n(r)$ (inset). For $\alpha = \beta$ this function takes a symmetric shape with a peak at $(r_{min} + r_{max})/2$. For the samples studied in this work we have chosen $\alpha = \beta = 3$ which corresponds to a distribution (solid line in Fig. 3) very close to a truncated Gaussian.

The width of the distribution is controlled by the polydispersity parameter δ_r which is defined as [23]:

$$\delta_r = \frac{r_{max} - r_{min}}{r_{max} + r_{min}}. \quad (9)$$

For $\delta_r = 0$ the particles are monodisperse while $\delta = 1$ corresponds to infinite polydispersity.

The shape of an ellipsoid is characterized by two parameters here defined as $\eta = a/b > 1$ and $\zeta = b/c > 1$, with $a \geq b \geq c$. For prolate ($a = b < c$) and oblate ($a = b > c$) ellipsoids, the shape can be fully characterized by the aspect

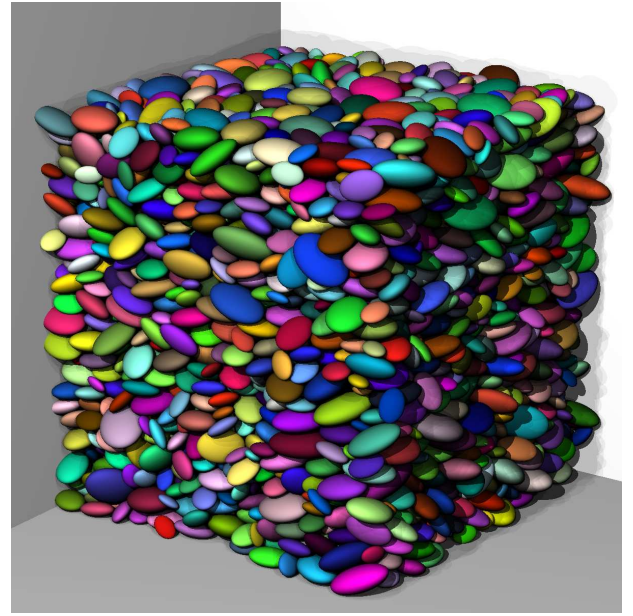


FIG. 4: (Color online) A deposit consisting of $N \sim 4200$ ellipsoids with shape parameters $\eta = 1.4$ and $\zeta = 1.8$ a polydispersity of $\delta_r = 0.6$, that is, $r_{min} = 0.016$ and $r_{max} = 0.064$ (see text). Colors are arbitrarily chosen for better visualization.

ratio $a/c = \eta\zeta$. The particular case $\eta = \zeta = 1$ corresponds to the sphere. These shape parameters together with the size $r > 0$ fully specify any ellipsoid.

Similar to the size polydispersity, two additional parameters δ_η and δ_ζ can be similarly defined for the polydispersities in the shape of the particles. In this study we consider systems of mono-shaped particles, describing each deposit by η , ζ and size polydispersity δ_r .

In this work, all the deposits are generated by releasing particles with randomly chosen positions and orientations and letting them fall in an open box, under gravity along the vertical direction. The box is limited from below by a rigid wall (ground) and is periodic in x and y directions. In order to reduce the boundary effects the first few bottom layers of particles are not considered in our analysis. Figure 4 shows a deposit of ellipsoidal particles with $\eta = 1.4$, $\zeta = 1.8$ and $\delta_r = 0.6$.

IV. MACROSCOPIC PROPERTIES OF THE DEPOSIT

The macroscopic properties considered in our study are the packing density, the average coordination number and the anisotropy.

A. Packing density and coordination number

Figure 5 shows the packing density in deposits of $N \sim 3000$ mono-disperse ellipsoids as a function of the shape. The

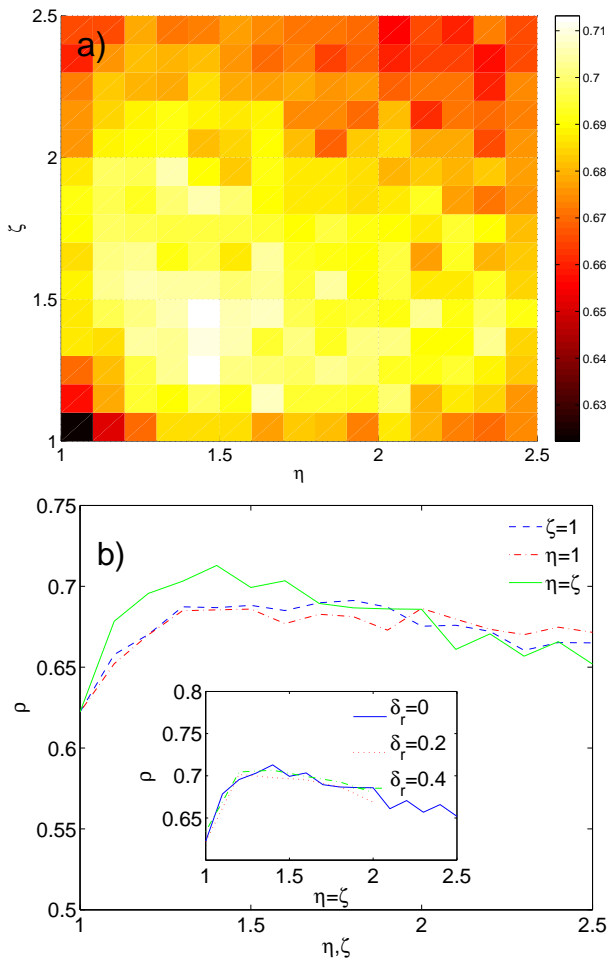


FIG. 5: (Color online) **(a)** Density ρ of monodisperse deposits as a function of the shape parameters η and ζ . The density is approximately symmetric with respect to the diagonal $\eta = \zeta$ where it attains a maximum. **(b)** The density as a function of shape along the diagonal $\eta = \zeta$ (solid line) together with the case of prolate ellipsoids ($\zeta = 1$, dashed line) and of oblate ellipsoids ($\eta = 1$, dashed-dotted line). In the inset the density is plotted as a function of $\eta = \zeta$ for different polydispersities δ_r . $N \sim 3000 - 4500$ depending on the amount of the size polydispersity.

immediate realization is that the density is to a large extent symmetric with respect to the axis $\eta = \zeta$.

When the shape deviates from the spherical shape, i.e. when $\eta > 1$ or $\zeta > 1$, the density first increases rapidly, then it attains a maximum and finally decreases slowly. From Fig. 5a one sees that typically, along lines of constant η (or constant ζ) the maximum is observed around $\eta = \zeta$. Further, along $\eta = \zeta$ a global maximum is attained at $\eta = \zeta \approx 1.4$, as can be observed from Fig. 5b (solid line). This absolute maximum curiously approximates the value of the golden ratio $(1 + \sqrt{5})/2$, which from the definition of η and ζ corresponds to when $a = b + c$. Whether such an observation is merely a coincidence or not needs further investigations which is out of the scope of our manuscript.

These results are qualitatively similar to those obtained in

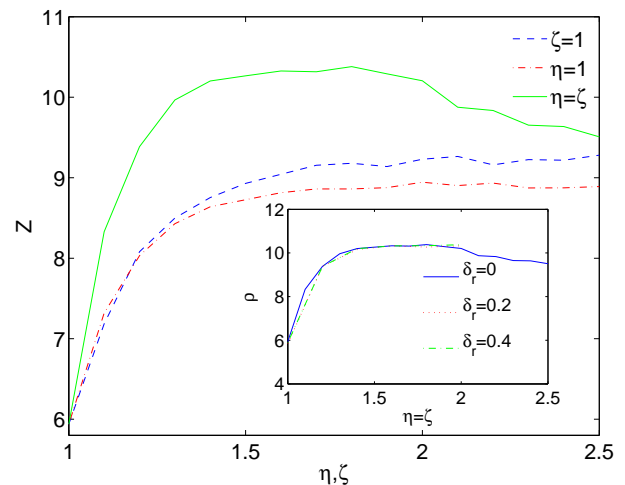


FIG. 6: The average coordination number as a function of the shape parameters η and ζ . Here $N \sim 3000$.

Refs. [13, 14] where a slightly higher density is observed, due to their method for generating the packings: instead of being generated via deposition, their samples are prepared in order to be in jammed state using a generalized form of Lubachevsky-Stillinger algorithm [28, 29].

The effect of polydispersity is examined by comparing the result for three different values of δ_r as shown in the inset of Fig. 5b. The results indicate that the density seems to be insensitive to low and moderate size polydispersities.

Figure 6 shows the average coordination number Z as a function of the shape of the particles. For spheroidal particles, Z increases gradually with the aspect ratios toward a maximum. For a general ellipsoid the coordination number attains a maximum higher than the maximum observed for spheroids ($\eta = 1$ or $\zeta = 1$), but decreases to values comparable to those of spheroids for larger η and ζ . This can be understood considering the fact that for $\eta = \zeta \gg 1$, one of the semi-axis radii is significantly larger than the other two and therefore the particle can be regarded as a prolate ellipsoid.

B. Anisotropy

To study the anisotropy of the deposits we investigate the orientational order of the contact vectors and the principal directions of the ellipsoids by calculating their angular distributions. In general two angles are needed to specify the orientation of a vector in three dimensional space, namely one azimuthal angle and one angle with the vertical direction. Our deposits are symmetric by construction in azimuthal direction. This is also observed in our results (not shown here for the sake of brevity). Therefore, we will only consider the angle with the positive vertical direction.

Figure 7a shows the results for deposits for different values of the shape parameters η, ζ where $\delta_r = 0$. The vertical axis, $P(\Omega(\theta))d\Omega$, represents the fraction of number of vectors

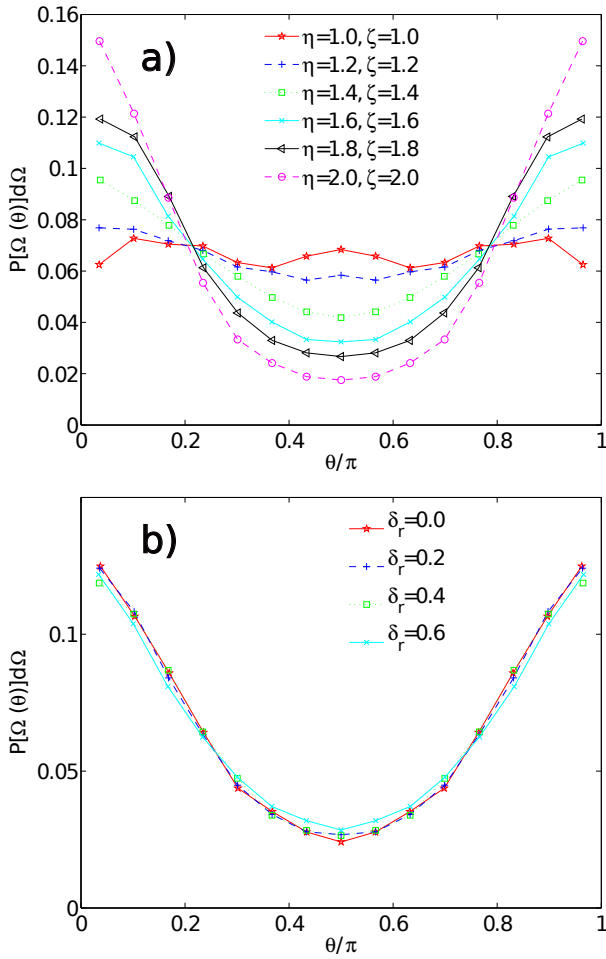


FIG. 7: The anisotropy of the contact normal. **(a)** Histogram of the angle θ between the contact vectors and the positive z -semiaxis for different shape parameters η and ζ , for the mono-sized case ($\delta_r = 0$). **(b)** Histogram of the angle θ for for a given shapen ($\eta = 1.6, \zeta = 1.8$) but different size polydispersity. Here $N \sim 3000 - 4500$ depending on the amount of the size polydispersity.

within the solid angle swept by a conic shell whose axis is parallel to z and its vertex angle is 2θ . Note that the curves are symmetric with respect to $\theta = \pi/2$ because for each contact normal of a particle there is a contact normal with opposite direction from the other particle to which it is in contact.

The results show that for deposits of spheres the distribution $P(\Omega(\theta))$ is independent of θ , and consequently the configuration of the contacts is isotropic and has no preferred direction. However, as the shape of the particles deviates from a sphere the number of side contacts between particles, i.e. the number of contacts on the horizontal plane, decreases and the contact normals line up along the vertical direction. This is seen in Fig. 7a which shows for each shape there is a minimum at $\theta = \pi/2$ which corresponds to the number of contacts on the (x, y) -plane, while having a maximum around $\theta = 0$ (vertical direction). The minimum at $\theta = \pi/2$ together with the maximum at $\theta = 0$ get more pronounced when increasing η and ζ .

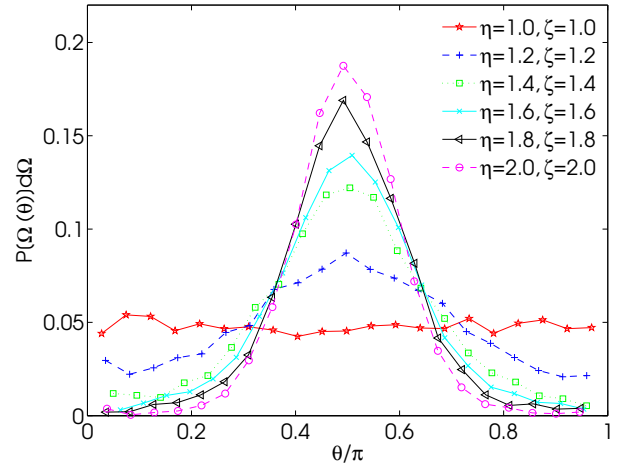


FIG. 8: Distributions of the orientation angle θ between the largest semi-axis \vec{a} of each particle and the positive z -semiaxis. Each curves corresponds to particular values of the shape parameters. Here $N \sim 3000$.

This means that for larger values of η and ζ which correspond to higher asphericities the particles tend to lie horizontally, for minimizing potential energy during deposition. Consequently most of the contacts will occur with the particles beneath and above. This can have dramatic effect on the force chains and the response of under shear and compression. Such a study is, however, beyond the scope the current work.

Figure 7a also shows two crossing points at a value slightly higher than $\theta \sim \pi/5$, indicating this direction as an invariant directions while varying the shape of the depositing particles.

Figure 7b shows the comparison of the angular distribution of contact normals for deposits with $\eta = 6, \zeta = 1.8$, with different polydispersities δ_r . It is clear that the polydispersity has a minor effect.

To study the anisotropy of the orientation of the particles we do a similar analysis for the principal directions of each ellipsoid. Figure 8 shows the results for the largest semi-axis \vec{a} for the deposits. One can see that as the shape of the particles deviates from a sphere the largest semi-axis \vec{a} also tends to lie on the (x, y) -plane. An invariant orientation is also observed, now for $\theta \sim \pi/3$. The polydispersities in the sizes of the particles has again no significant effects on the orientation anisotropy (not shown).

V. CONCLUSIONS

In this work, we studied systematically the static properties of deposits composed of ellipsoidal particles of different size and shape, focusing on their density and anisotropy. To this end, we developed an efficient Molecular Dynamics method for simulation of ellipsoidal particles which we used to generate deposits of such particles under gravity.

For mono-sized particles, the density increases rapidly as the shape of the particles deviates from a sphere, reaching for

particular values of the shape parameters a maximum significantly higher than the one observed in random close packing of spheres. With increasing further the shape parameters, that is, deviating further for a sphere density to decrease slowly. The densities observed in the deposits are generally lower than the ones obtained through procedures for optimal packings. Thus, as expected, deposition is not an ideal process for achieving the largest densities. Typically, porous media and media formed through deposition processes present also densities much lower than the optimal one. Such observations point toward the possibility for using deposition of ellipsoids as a proper procedure for modeling porous media. This is the subject of future works.

In the case of polydisperse particles the density takes higher values with qualitatively similar behavior. A rather unexpected result is that the polydispersity in the sizes of the par-

ticles has almost no effect on the anisotropic behavior of the system.

We also study the anisotropy of such deposits and show that as the shape of the particles deviates from a sphere stronger anisotropies are observed. Such anisotropies appear due to the gravity and are absent in the systems without gravity.

Acknowledgements

The authors thank Bibhu Biswal and Jens Harting for useful discussions and the *Fundação para a Ciência e a Tecnologia* for financial support, under the fellowship *SFRH/BPD/48974/2008* and contract *Ciência 2007*.

-
- [1] S. Torquato and F.H. Stillinger, *Rev. Mod. Phys.* **82** 2633 (2010).
 - [2] D. Kadau and H.J. Herrmann, *Phys. Rev. E* **83** 031301 (2011).
 - [3] R.C. Hidalgo, D. Kadau, T. Kanzaki, H.J. Herrmann, "Granular packings of cohesive elongated particles", arXiv: 1107.3040 (2011).
 - [4] A.S. Joshi and Y. Sun, *Phys. Rev. E* **82** 041401 (2010).
 - [5] B. Biswal, R.J. Held, V. Khanna, J. Wang, and R. Hilfer, *Phys. Rev. E* **80** 041301 (2009).
 - [6] M. Bloom, M. Russel, A. Kustau, K. Muriel, S. Mandayam, B. Sukumaran, *Powders and Grains 2009*, Proc. 6. Int. Conf. on Micromechanics of Granular Media (AIP, 2009), pp. 195-198 and references therein.
 - [7] J.J. Schneider, A. Müller, E. Schömer, *Phys. Rev. E* **79** 031122 (2009).
 - [8] S.D.S. Reis, N.A.M. Araújo, J.S. Andrade Jr., H.J. Herrmann, "How dense can one pack spheres of arbitrary size distribution?", preprint, available at arXiv:1109.0966 (2011).
 - [9] R. Mahmoodi Baram, H.J. Herrmann, and N. Rivier, *Phys. Rev. Lett.* **92** 044301 (2004).
 - [10] R. Mahmoodi Baram and H.J. Herrmann, *Phys. Rev. Lett.* **95** 224303 (2005).
 - [11] P.G. Lind, R.M. Baram, H.J. Herrmann *Phys. Rev. E* **77** 021304 (2008).
 - [12] A. Donev, I. Cisse, D. Sachs, E.A. Variano, F.H. Stillinger, R. Connelly, S. Torquato, P.M. Chaikin, *Science* **303**(5660), 990-993 (2004).
 - [13] A. Donev, R. Connelly, F.H. Stillinger, S. Torquato, *Phys. Rev. E* **75** 051304 (2007).
 - [14] G.W. Delaney and P.W. Clearly, *Europhys. Lett.* **89** 34002 (2010).
 - [15] Y. Jiao, F.H. Stillinger and S. Torquato, *Phys. Rev. Lett.* **100** 245504 (2008).
 - [16] T. Pöschel and T. Schwager, *Computational Granular Dynamics* (Springer, Berlin, 2005).
 - [17] D.C. Rapaport, *The Art of molecular dynamics simulation*, (Cambridge University Press, Cambridge, 1995).
 - [18] J.W. Perram and M.S. Wertheim, *J. of Comp. Phys.* **58**, 409-416 (1985).
 - [19] J.W. Perram, J. Rasmussen, E. Præstgaard, J.L. Lebowitz, *Phys. Rev. E* **54**, 6565-6572 (1996).
 - [20] P.G. Lind *in* *Powders and Grains 2009*, Proc. 6. Int. Conf. on Micromechanics of Granular Media (AIP, 2009), pp. 219-222.
 - [21] X. Lin and T.-T. NG, *Int. J. Num. Anal. Meth. Geomech.* **19** 653-659 (1995).
 - [22] N.V. Brilliantov, F. Spahn, J.-M. Hertzsch, and T. Pöschel, *Phys. Rev. E* **53** 5382 (1996).
 - [23] C. Voivret, F. Radjaï, J.-Y. Delenne, and M. S. El Youssoufi, *PRE* **76**, 021301 (2007).
 - [24] M.P. Allen, G.T. Evans, D. Frenkel and B.M. Mulder, *Hard Convex Body Fluids*, Adv. Chem. Phys. **LXXXVI** (Ed. I. Prigogine and S.A. Rice, John Wiley, 1993).
 - [25] W. Wang, Y.-K. Choi, B. Chan, M.-S. Kim and J. Wang, *Computing* **72** 235 (2004).
 - [26] G.J. Semple and G.K. Kneebone, *Algebraic projective geometry* (Oxford Univ. Press, London, 1952).
 - [27] J.M. Tavares, M. Tasinkevych, F. de los Santos, M.M. Telo da Gama, *Molecular Physics* **101** 1659 (2003).
 - [28] B.D. Lubachevsky, F.H. Stillinger, *J.Stat.Phys.* **60**, 561 (1990).
 - [29] B.D. Lubachevsky, F.H. Stillinger, E.N. Pinson, *J.Stat.Phys.* **64**, 501 (1991).